Fragment-based optimized EthR inhibitors with in vivo ethionamide boosting activity

Baptiste Villemagne[†], Arnaud Machelart[‡], Ngoc Chau Tran[†], Marion Flipo[†], Martin Moune[‡], Florence Leroux[†], Catherine Piveteau[†], Alexandre Wohlkönig[+], René Wintjens[α], Xue Li[=], Ruxandra Gref[=], Priscille Brodin[‡], Benoit Deprez[†*], Alain R Baulard[‡], Nicolas Willand[†]*

†Univ. Lille, Inserm, Institut Pasteur de Lille, U1177—Drugs and Molecules for Living Systems, F-59000 Lille, France; ‡Univ. Lille, CNRS, Inserm, CHU Lille, Institut Pasteur de Lille, U1019-UMR8204-CIIL–Center for Infection and Immunity of Lille, F-59000 Lille, France; +Structural Biology Brussels and Molecular and Cellular Interactions, VIB, Brussels, Belgium; α Unité Microbiologie, Bioorganique et Macromoléculaire (CP206/04), Institut de Pharmacie, Université Libre de Bruxelles, Brussels, Belgium; =Univ. Paris Sud, Univ. Paris-Saclay, CNRS, UMR 8214 - Institute for Molecular Sciences of Orsay (ISMO), Orsay, France.

*To whom correspondence should be addressed. Phone: +33 (0)320 964 991. Fax: +33 (0) 320 964 709. E-mail: baptiste.villemagne@univ-lille.fr.

Home pages: U1177, http://www.deprezlab.fr

ABSTRACT. Killing more than one million people each year, tuberculosis remains the leading cause of death from a single infectious agent. The growing threat of multidrug resistant strains of *Mycobacterium tuberculosis* stresses the need for alternative therapies. EthR, a mycobacterial transcriptional regulator, is involved in the control of the bioactivation of the second-line drug ethionamide. We have previously reported the discovery of *in vitro* nanomolar boosters of ethionamide through fragment-based approaches. In this study, we have further explored the structure-activity and structure-property relationships in this chemical family. By combining structure-based drug-design and *in vitro* evaluation of the compounds, we identified compound **27** (**BDM71339**), the first fragment-based ethionamide booster which proved active *in vivo*, in an acute model of tuberculosis infection.

Introduction

Tuberculosis (TB) remains a major global health problem, and is today the first leading cause of death from a single infectious disease worldwide. According to the WHO 2018 report, there were 10.0 million new TB cases in 2017 and 1.6 million deaths due to TB infection[1]. After more than 40 years of neglected antituberculosis drug development, the pipeline has recently been filled promisingly with repurposed old drugs, or with new chemical entities such as bedaquiline and delamanid.[2, 3] In parallel, we developed an alternative strategy to reinforce the therapeutic armamentarium against TB, by designing drug-like molecules that boost the bioactivation of ethionamide (ETH), a second-line antitubercular drug, in order to enhance its efficacy.[4, 5]

A fragment-based approach to foster the discovery of potent EthR inhibitors.

ETH is a second-line drug widely used in the treatment of multidrug-resistant TB (MDR-TB). Like many other anti-TB drugs, ethionamide is a prodrug. It is bioactivated inside the mycobacteria by the flavin-containing monooxygenase EthA into an ethionamide-NAD adduct.[6] This active ethionamide-NAD complex inhibits the synthesis of mycolic acids by targeting InhA. It is now well known that a mycobacterial transcriptional repressor belonging to the TetR family of transcription factors, called EthR, controls EthA expression and thus limits ethionamide bioactivation and activity.[7, 8]

We previously demonstrated that inhibiting EthR with small molecules strongly increases the sensitivity of the pathogen to ethionamide both *in vitro* and *in vivo*, thus validating EthR as a new drug target to fight TB.[4] This discovery was reinforced by the identification of two different families of EthR inhibitors using structure-based design and high-throughput screening.[9-11]

The development of lead compounds in the field of infectious diseases through fragment-based drug design (FBDD) approaches have become more and more popular in medicinal chemistry to discover lead compounds and develop clinical candidates in the last decades.[12-14] Indeed, owing to their small size and low molecular weight, fragment usually display better physicochemical properties, especially solubility, than lead-like or drug-like compounds, which makes them attractive in the aim of penetrating the thick and poorly permeable Mtb cell envelope.[15] As an exemple, structure-guided fragment-linking and growing approaches were used by Surade, Nikiforov *et al.* to generate potent *in vitro* ethionamide boosters.[16-18] Chan *et al.* used native electrospray ionization-mass spectroscopy (ESI-MS) to study the interactions and stoichiometry

of EthR/DNA (62 bp) complexes[19] and to screen fragments[20], leading to the discovery of two able to disrupt EthR-DNA interaction in the high micromolar range.

Our group has combined surface plasmon resonance (SPR) and X-ray crystallography, to identify compound **1** (Figure 1) as new chemotype of EthR ligand.[21] Optimization of fragment **1** using fragment growing, merging and linking strategies led to several potent ethionamide boosters. Out of these, compound **2** (Figure 1) coming from a fragment—growing strategy, was the most promising inhibitor and was further optimized into compound **3** (Figure 1, **BDM43266**) which is able to boost ten times the activity of ethionamide in TB-infected macrophages at low nanomolar concentrations (EC_{50} = 0.10 μM).[21]

Fragment **1** and optimized analog **3** have previously been cocrystalized with EthR (Figure 2).[21] Two molecules of fragment **1** occupy the long and linear ligand binding domain of EthR. One molecule, in the bottom of the pocket, is hydrogen-bonded to the side chain of Asn179 and π-stacked with the phenyl ring of Phe110. The second molecule, located at the portal of the cavity, is positioned to fill the two hydrophobic pockets D2 and D2', while H-bonded to Tyr148 and π-stacked with Trp103 in a T-shaped manner. Compound **3** binds tightly to EthR through a new binding mode by creating hydrogen bonds with the two Asn179 and Asn176. The methylthiazole motif points towards the two upper pockets D2 and D2', delimited by hydrophobic residues and the side chain of Tyr148. In the crystal structure of EthR liganded by compound **3**, D2' is occupied by the flexible methionine 102.

In our previous work, we mainly focused our structure-activity relationships study on the modifications of the (sulfon-)amide chain, responsible for the H-bonding of the inhibitors to the

protein. In order to further improve the potency of our ligands, we herein started to explore substitution of the positions 5 and 2 of the thiazole ring (compounds **4-14**) in order to occupy pockets D2 and D2'. These modifications were found to impact negatively the physicochemical properties. This was counterbalanced by replacing the thiazole ring with other 5-membered heterocycles (compounds **15-21**), and by replacing the phenyl ring with pyridines (compounds **22-23**). As previously described, the compounds were ranked based on their potency (EC_{50}) as well as the calculated ligand efficiency (LE = (1.37*pEC_{50})/(HAC) ; HAC: Heavy Atoms Count).[21] At this stage, physicochemical and pharmacokinetic properties of the most active and efficient compounds were determined and compared in order to select the most appropriate compound for *in vivo* validation. An issue that we had to take into account is that our compounds displayed a low microsomal stability. This drawback was partially overcome by replacing the oxidizable methyl substituent on the 5-membered heterocycle with more metabolically stable moieties (compounds **24-28**), leading to the discovery of compound BDM71339 (**27**) which displays improved physicochemical properties and microsomal stability suitable to allow the boosting of ethionamide's activity in a mouse model of TB infection.

Chemistry

We started to explore new structure-activity relationships by halogenating the thiazole ring (compounds **4-5**). The fluorinated thiazole **4** was obtained by direct fluorination of compound **3** using Selectfluor in DMF[22] (Figure 3). The chlorinated analog **5** was obtained starting from 4-(2-methylthiazol-4-yl)-benzoic acid, that was first refluxed into thionyl chloride to give the corresponding acyl chloride chlorinated in position 5 of the thiazole ring. Coupling with 3,3,3-trifluoropropylamine led to the desired compound **5**.

In order to further improve the potency of our ligands, we explored the substitution of the methyl in position 2 of the thiazole ring. As previously mentioned this methyl points towards the two hydrophobic pockets D2 and D2' and the side chain of Tyr148. We thus sought to introduce aliphatic and aromatic substituents that could occupy one of the two pockets D2 and D2' (compounds **6**-**13**), and potentially be hydrogen-bonded to Tyr148 as fragment **1**. To that purpose, we substituted the methyl group on the thiazole ring with H-bond acceptor moieties such as esters (ethyl (**6**) or isopropyl (**7**)) and a 2-methylpropane-2-sulfonyl moiety (**8**), or with purely hydrophobic alkyl chains (compounds **12** and **13**). In parallel, we investigated the direct substitution of the thiazole ring with ethyl ester (**9**), isopropyl ester (**10**) and 4-pyridine ring (**11**) (Figure 4**.**).

The synthesis of these analogs followed a similar pathway (Figure 4**.**). 4-acetylbenzoic acid was coupled to 3,3,3-trifluoropropylamine to give the ketone **6a** which was then brominated, leading to the bromoketone **6b**. Condensation with synthesized (see supporting information) or commercially available thioamides led to the desired substituted thiazoles (**8, 9, 11-13**). Esters **6** and **7** were obtained from the cyano derivative **6c** by reaction with ethanol and 2-propanol respectively in the presence of trimethylsilyl chloride. Conversion of the ethyl ester **9** into the desired isopropylic analog **10** also led to the decarboxylated product **14**.

Further modifications were performed by replacing the thiazole ring with other 5-membered heterocycles (compounds **15-21**) or by changing the phenyl ring for a pyridine ring (compounds **22-23**).

As for the thiazole-based compounds, the oxazole analog (**15**) was obtained by condensation of the bromoketone **6b** and acetamide (Figure 5). 1,2,4 oxadiazoles **16** and **17** were obtained in 3 steps starting from 4-cyanobenzoic acid and terephthalic acid monomethyl ester respectively, which were coupled with 3,3,3-trifluoropropylamine to give intermediates **16a** and **17a**. The cyano derivative **16a** was reacted with hydroxylamine to produce amidoxime **16b,** which was further cyclized with acetic acid into the 1,2,4-oxadiazole **16**.[23] The ester **17a** was hydrolyzed to the corresponding carboxylic acid **17b** which was reacted with acetamide oxime to give the 1,2,4-oxadiazole **17**. Condensation of the carboxylic acid **17b** with acetyl hydrazine also led to the 1,3,4-oxadiazole analog **18**. The 1,3,4-thiadiazole analog **19** was obtained in 3 steps. First, the 1,3,4-thiadiazole ring was formed by reacting together 4-cyanobenzoic acid, acetyl hydrazine, T3P and Lawesson's reagent.[23] Basic hydrolysis of the nitrile moiety and coupling with 3,3,3-trifluoropropylamine led to the desired 1,3,4-thiadiazole **19**. The 1,2,4-triazole analog **20** was obtained from the previously synthesized intermediate **16a** which was reacted with methanol in the presence of HCl to give the benzimidic acid methyl ester intermediate. Condensation with acetyl hydrazine led to the desired 1,2,4-triazole **20**. Finally, the 1,2,3-triazole analog was obtained in 2 steps. 4-azidobenzoic acid was first coupled to 3,3,3-trifluoropropylamine and then reacted with 4-methyl-pentyne in a Huisgen 1,3-cycloaddition reaction to give the desired 1,2,3-triazole analog **21**.

The pyridine analogs **22** and **23** were synthesized in 3 and 4 steps respectively (Figure 6). Synthesis of **22** started from 5-bromo-pyridine-2 carboxylic acid coupled with 3,3,3-

trifluoropropylamine. Introduction of the methylketone moiety was then performed using a Stille coupling followed by acidic hydrolysis[24], leading to intermediate **22b**. Bromination and cyclisation with thioacetamide finally gave the desired compound **22**. Synthesis of the isomer **23** followed a similar pathway, starting from the coupling of 6-chloro-nicotinoyl chloride with 3,3,3-trifluoropropylamine to give the amide intermediate. Substitution of the chlorine atom with an iodine using NaI in acetonitrile[25] and introduction of the metylketone moiety as previously mentioned followed by bromination and cyclisation with thioacetamide led to the desired thiazole **23**.

Trifluoromethylated compounds **24-26** were synthesized as previously described for the methyl analogs, using the appropriate trifluoromethylated thioamide or carboxylic acid (Figure 7). Finally, oxadiazoles **27** and **28** were synthesized as previously described by reacting amidoxime **16b** with cyclopropanecarboxylic acid and isobutyric acid respectively.

Results and Discussion

We report herein the exploration of structure-activity relationships starting from compound **3** that we previously identified through a fragment-growing strategy.[21] The aim of this study was to try to increase the potency of our inhibitor while maintaining a low molecular weight (MW < 400g.mol^{-1}) and good physicochemical and pharmacokinetic properties suitable for an *in vivo* study. Compounds **4-28** were evaluated in two different assays, as previously reported.[21] Firstly, a thermal shift assay was used to evaluate their affinity for the EthR repressor. In this assay, a shift in the melting temperature between the holo and apo-EthR, expressed as ΔT_m, is measured and correlates with the affinity of the ligand for EthR. In a secondary assay, compounds are tested in a dose-ranging experiment in the presence of GFP-*M.tuberculosis* and a fixed inactive

concentration of ethionamide (0.1 µg/mL = MIC_{99}/10). The potency of the molecules to boost ten times the activity of ethionamide is reported as EC_{50}. This secondary assay also allows us to determine whether tested compounds show some antibacterial activity by themselves. In parallel, we calculated the ligand efficiency index (LE=(1.37*pEC_{50})/(HAC)) for all the compounds, in order to appreciate the effectiveness of each chemical modification on the activity.

The reference compound **3** bearing a methyl group on position 2 of the thiazole ring displays an EC_{50} of 0.10 µM and a ΔT_m of 10.6°C. First, we decided to explore the introduction of halogen atoms in position 5 of the thiazole ring. Introduction of a fluorine atom (compound **4**, EC_{50} = 55 nM) increased the activity while maintaining a high ligand efficiency (LE = 0.45). On the contrary, replacement with a chlorine atom (compound **5**) decreased the affinity for EthR (ΔT_m = 8.7°C) and was detrimental for the activity (EC_{50} > 2.5 µM). This is in agreement with the binding mode of compound **3** to EthR. Indeed, the thiazole ring occupies a very narrow tunnel, which could explain why only small substituents are allowed in this position.

We then decided to explore the substitution on position 2 of the thiazole. The non-substituted analog (compound **14**) showed less affinity for EthR (ΔT_m = 8.1°C) and was not able to boost ethionamide activity (EC_{50} > 2.5 µM) suggesting that a substituent on this position is required.

As aforementioned, to improve the activity we tried to occupy one of the two pockets D2, D2' and interact with Tyr148 side chain by introducing aromatic or aliphatic moieties bearing an H-bond acceptor atom in position 2 of the thiazole ring. Introduction of an ethoxycarbonylmethyl group (compound **6**, ΔT_m = 10.1°C, EC_{50} = 0.58 µM) led to a decrease of the potency whereas a bulkier ester (compound **7**, ΔT_m = 13.2°C, EC_{50} = 0.10 µM) restored activity. However, LE was lower compared to compound **3**. Replacement of the methyl group by a tert-butylsulfonylmethyl

group only slightly reduced the activity (compound **8**, EC_{50} = 0.25 µM) showing that ester and sulfonyl functions are tolerated in this position. Surprisingly, the direct connection of ester groups on the thiazole ring (compounds **9** and **10**) proved to be detrimental for the activity (EC_{50} > 2.5 µM). Finally, introduction of a pyridine ring (compound **11**, ΔT_m = 12.6°C, EC_{50} = 72 nM) slightly improved the activity but decreased the ligand efficiency (LE = 0.38). Globally, even if an increase of ΔT_m could be observed for some of the new analogs (compounds **7** and **11**) compared to reference compound **3**, our efforts to establish a new H-bond with Tyr148 did not lead to an improved potency. Therefore, we decided to introduce aliphatic chain to occupy pockets D2 or D2'. Introduction of an isohexyl substituent led to compound **12** which showed an excellent affinity for EthR (ΔT_m = 13.0°C) but was less potent (EC_{50} = 0.43 µM). Interestingly, a shorter isobutyl chain (compound **13**) increased both the affinity and the potency (ΔT_m = 12.6°C, EC_{50} = 49 nM) compared to compound **3**, while keeping a good LE (LE=0.42).

From this first series of analogs, compounds **4** and **13** were the only two to show a better potency than compound **3**, with a LE > 0.4. Compound **13** was cocrystallized with EthR (Figure 8). The X-ray structure revealed that compound **13** binds EthR through H-bonds with Asn176 and Asn179, and is π-stacked with Phe110 and Trp207 in a similar way than compound **3**. The moving of the flexible Met102, allows the isobutyl chain to occupy the D2' pocket.

At this stage, we evaluated the physico-chemical properties of our most potent analogs **3**, **4** and **13** (**Table 2**).

Introduction of a fluorine atom in position 5 of the thiazole (compound **4**) led to a compound as soluble as compound **3** (10.6 µg/mL) whereas the replacement of the methyl group of compound **3** by an isobutyl chain (compound **13**) increased the lipophilicity (logD = 3.9) and was thus detrimental for the solubility (1.6 µg/mL). In order to improve this property, we explored isosteric replacement of the thiazole ring by other 5-membered aromatic rings and replacement of the phenyl ring by a pyridine ring. From this point in the optimization, all new analogs have comparable size and HAC. Therefore, EC_{50} is directly correlated to LE and will be considered as the only selection criterion.

Replacement of the thiazole ring (Table 3) with 1,3,4-oxadiazole (compound **18**), 1,3,4-thiadiazole (compound **19**), 1,2,4-triazole (compound **20**) or 1,2,3-triazole (compound **21**) led to less potent compounds (EC_{50} > 2.5 µM). Exchange of the sulfur atom by an oxygen atom led to the 1,3-oxazole analog (compound **15**, EC_{50} = 0.28 µM) which displayed a slightly decreased activity. Similar potency was obtained with the 1,2,4-oxadiazole analog **17** (EC_{50} = 0.26 µM). Interestingly, the regioisomer, compound **16**, showed a slightly improved activity and a similar LE (EC_{50} =82 nM and LE = 0.46) than compound **3**.

Finally, modifications of the central phenyl ring were performed (**Table 4**). Introduction of a pyridine ring with the nitrogen atom adjacent to the amide linker (compound **22**, EC_{50} = 0.17 µM) did not impact the activity significantly, whereas activity seriously dropped when the nitrogen atom is adjacent to the thiazole ring (compound **23**, EC_{50} = 1.0 µM).

At this stage, in order to bring out a compound for *in vivo* experiments, we selected the best analogs (**3**, **16**, **22**) for further physicochemical and mouse liver microsomal stability evaluation (**Table 5**).

As expected, replacement of the thiazole ring with a 1,2,4-oxadiazole led to a decrease of the lipophilicity (compound **16**, logD = 2.3) and a slight increase in solubility (21.8 µg/mL). This increase of solubility was more pronounced when replacing the phenyl ring by a pyridine ring (compound **22**, 61.1 µg/mL).

However, the selected compounds displayed poor microsomal stability ($t_{1/2}$ < 10 min, Cl >100 $\mu L.min^{-1}.mg^{-1}$). The major metabolite identified from compound **3** was the corresponding alcohol **3'**. We did not observe the formation of carboxylic acid **3''** (Figure 9).

Compound **3'** was however less active (EC_{50} = 0.73 µM, LE = 0.39) than the reference compound **3**. We therefore decided to replace hydrogen atoms with fluorine atoms to avoid oxidation of the methyl moiety, and thus increase the metabolic stability (compounds **24**-**26**). Interestingly, this substitution did not negatively impact the activity since compound **24** (EC_{50} = 0.10 µM, **Table 6**), was found as potent as compound **3**. The same tendency was observed for **25** and **26** *versus* **22** and **16** respectively. Ligand efficiency was lower for the trifluoromethylated compounds (0.40 < LE < 0.41) compared to their methyl analogs (LE ≥ 0.44) but was nonetheless maintained to a substantially high level.

We previously observed that small alkyl chains were well tolerated in position 2 of the thiazole. Therefore, we also replaced the methyl moiety with potentially more metabolically stable alkyl substituents.[26] The cyclopropyl (compound **27**, EC_{50} = 0.072 µM) and the isopropyl (compound **28**, and EC_{50} = 0.065 µM) analogs, both displayed equivalent potency as the reference compound **16**.

The solubility, logD and microsomal stability of compounds **24** to **28** were measured (**Table 6**). The modifications of the substituent on the heteroaromatic ring led to more lipophilic compounds (3.1 < logD < 3.6) which did not allow to improve the solubility (2.4 < solubility < 17.2 µg/mL).

However, as expected, fluorination of the methyl group led to more stable compounds (compounds **24-26**, 16 < $t_{1/2}$ < 22 min). Introduction of an isopropyl group (compound **28**, $t_{1/2}$ = 6 min) did not help to metabolically stabilize the 1,2,4-oxadiazole analog whereas introduction of a cyclopropyl group (compound **27**, $t_{1/2}$ = 19 min) led to an increase in the stability.

At this stage, we decided to evaluate the ability of a set of EthR inhibitors to boost the activity of ethionamide in a mouse model of *M. tuberculosis* infection. We recently used an aerosol pulmonary administration of poly-β-cyclodextrin nanoparticles (pCD) co-loaded with ETH and **BDM41906**, the lead compound from our structure-based design derived family, for the treatment of TB infected mice.[27] Of note, monomeric β-CD is widely used to solubilize a variety of drugs and to improve their bioavailability.[28] The use of biodegradable polymeric pCD allowed to overcome the issues of low water solubility of both the booster and ETH, in order to directly administrate the anti-TB combo into the lungs, the major infection site of *M. tuberculosis*, thanks to microsprayer. This formulation was shown to be much more efficient than the oral gavage of the same cocktail, since the treatment of infected mice with six doses of pCD loaded with the two drugs (50 µL containing 4 mg/mL of ETH and 4 mg/mL of **BDM41906** co-loaded in 200 mg/mL of pCD) led to a 2 log decrease of the pulmonary bacterial load. On top of that, we also have demonstrated that compound **3** can be co-encapsulated with ETH in pCD, leading to a 90-fold increase in the apparent solubility of the booster.[29] Interestingly, pCD allowed for an

efficient one-step incorporation of both ETH and the booster by a solvent-free "green" procedure.

Therefore, we selected compounds **24-27** (compounds with EC_{50} < 100 nM and Cl < 80 µg.ml/min) for co-encapsulation with ETH in the presence of pCD. Surprisingly, only compound **27** (**BDM71339**) could be solubilized at a concentration high enough (4 mg/mL) required to test the ETH-booster pair at 10 mg/kg of each compound in the presence of 200 mg/mL pCD in water. We investigated the ability of the co-encapsulated ETH-**27** pair to reduce the pulmonary mycobacterial load in an acute *in vivo* model of TB infection. BALB/c mice were intranasally infected for 7 days before being treated for 2 weeks, with 6 endotracheal administration of spay of the ETH-booster loaded pCD at 10 mg/kg of each compound using a microsprayer (Figure 10).

The two weeks treatment with the ETH-**27** pair led to a reduction of the pulmonary bacterial load of more than 2 log units ($P < 0.001$) in comparison to the control (untreated) group, to a level comparable to day 0. It should be noted that the reduction of the bacterial load obtained with the combination was higher than when ETH was administrated alone. This boosting effect was equivalent to the one obtained with our reference booster **BDM41906**.

Conclusion.

We extensively studied the structure-activity relationships around **BDM43266** (compound **3**), a nanomolar ethionamide booster identified through a fragment based approach, by exploring the replacement of the core phenyl ring by pyridines, the substitution of the positions 5 of the thiazole by halogen atoms, the isosteric replacement of the thiazole ring with other 5-membered heterocycles and the introduction of diverse substituents in the position 2 of this thiazole ring. One of the challenges was to improve the microsomal stability of the lead compound while maintaining acceptable activity and efficiency. Modifications with a huge impact on molecular weight and heavy atom count never led to a significant improvement of the activity but were however detrimental for the physicochemical properties. On the contrary, subtle modifications such as replacing the 2-methylthiazole with a 2-cyclopropyloxadiazole (compound **27**, **BDM71339**) led to a potent EthR inhibitor with improved microsomal stability. This compound was also able to boost ethionamide activity at low nanomolar concentrations *in vitro*. Finally, when co-administered with ETH in a mouse model of acute *M. tuberculosis* infection, **BDM71339** was able to boost significantly ETH activity. The use of pCD nanoparticle-based formulation allowed drug administration directly into the lung to target more rapidly and more efficiently the bacteria at the site of infection to bypass limitations for some current TB drugs of oral treatment and reduce systemic side effects. Noteworthy, drugs were spontaneously associated to the NPs in the absence of organic solvent.

This work is the first reported example of fragment-based EthR inhibitors with *in vivo* ethionamide boosting efficacy, therefore validating the use of fragment-based approaches for the development of bacterial transcriptional repressor inhibitors.

Experimental section

Biology.

Thermal shift assay (TSA). The fluorescent dye SYPRO Orange (Invitrogen) was used to monitor protein unfolding. The thermal shift assay was conducted in a Lightcycler 480 (Roche). The system contained a heating/cooling device for temperature control and a charge-coupled device (CCD) detector for real-time imaging of the fluorescence changes in the wells of the microplate. The final sample concentrations were 10 μM EthR, 2.5X SYPRO Orange, 1% DMSO and 20 μM ligand in the EthR buffer. The samples were heated from 37 to 85 °C with a heating rate of 0.04 °C/sec. The fluorescence intensity was measured at Ex/Em: 465/510 nm. The data were obtained using the algorithmic program Wavemetrics Igor by applying the following designed procedure: the fluorescence intensity of each well/sample is plotted as a function of the temperature. Then, the 1D-numerical derivative of these curves is calculated. At last, the maximum data values, corresponding to the inflection points (Tm), is extracted to give Tm in a table and in a graph.

Potency assay of test compounds on *M. tuberculosis* (ethionamide concentration fixed at 0.1 μg/mL, serial dilution of test compounds). Ethionamide (Sigma E6005-5G) is diluted into DMSO to 10 mg/mL and aliquots are stored frozen at -20 °C. Test compounds are suspended in pure DMSO at a concentration of 40 mg/mL in Matrix tubes and then diluted by a ten-fold dilution to 4 mg/mL in eppendorf tubes. Ten 2-fold serial dilutions of compounds are performed in DMSO in Greiner 384 well V-shape polypropylene plates (Greiner, #781280). Equal volumes (5 μL) of diluted compounds and of ethionamide are transferred to a 384-well low volume polypropylene plate (Corning, #3672). Two independent replicates were done for each setting.

On the day of the experiment, 0.5 µL of compound-plate is first transferred by EVOBird platform (Evotec) to cell assay plates pre-plated with 10 µL of assay medium.

pCD preparation. βCyD was kindly supplied by Roquette, Lestrem, France. pCD nanoparticles of around 10 nm were produced as previously described[21] by crosslinking β-CyD under strongly alkaline conditions with epichlorohydrin. Encapsulation of ETH and Booster in pCD nanoparticles was carried on without using any organic solvent, by mixing for at least 4 hours at 37°C the NP suspensions with the drug powders.

Mice. 6-week old Balb/C female mice were purchased from Janvier (Le Genest-Saint-Isle, France) and were maintained in the animal house facility of the Pasteur Institute of Lille, France (Agreement B59-350009). The project received ethical approval by French Committee on Animal Experimentation and the Ministry of Education and Research (00579.01 approved on December 2nd, 2015) and all experiments were performed in accordance with relevant guidelines and regulations.

Mice infection and treatment. 8-week-old mice (4 mice *per* group) were inoculated with *M. tuberculosis* H37Rv via the intranasal route (10^5 CFU/20 µl) as previously described[18] .Treatment administrations were performed on day 7, 9, 11, 14, 16 and 18. Briefly, mice were placed in isoflurane chamber (Aerrane®, Baxter SAS, France). Each mouse was placed on the back on a platform (Mouse Intubation Platform – Model MIP, Penn Century Inc., Wyndmoor, PA) with isoflurane mask and hanging on its teeth. The tongue was pulled out by a tweezer and a laryngoscope (Small Animal Laryngoscope for mouse– Model LS-2-M, Penn Century Inc., Wyndmoor, PA) was used to see the trachea and to enable the aerosolization of 50 µL of

nanoparticle suspensions (ETH, ETH + BDM41906 or ETH + 27) inside the lungs. Briefly, 50 µl of water containing pCD loaded with (or PBS alone as control) were administered to mice via the endotracheal route using a Microsprayer® (MicroSprayer® Aerosolizer – Model IA-1C-M and FMJ-250 High Pressure Syringe, Penn Century Inc., Wyndmoor, PA). At day 21, mice were euthanized and lungs were homogenized with MM300 bead beater (Retsch) and ten-fold serial dilutions were plated onto 7H11 agar plates supplemented with 10% OADC. CFUs were determined after a three-week growth at 37 °C. Statistics were performed using Student's t-test analysis. Comparison of groups two-by-two was performed and the results are displayed when required. Values of $p < 0.05$ were considered to represent a significant difference. **, and *** denote $p < 0.01$, and $p < 0.001$, respectively

ADME studies.

These experiments were analyzed using a LC-MS-MS triple-quadrupole system (Varian 1200ws) under SIM or MRM detection with optimized mass parameters (declustering potential; collision energy and drying gas temperature).

LogD. 40 µL of a 10 mM solution in DMSO of the compound was diluted in 1.960 mL of a 1/1 octanol/PBS mixture at pH 7.4. The mixture was gently shaken for 2 h at room temperature. Ten microliters of each phase was diluted in 490 µL of MeOH and analyzed by LC-MS/MS. Each compound was tested in triplicate. Log D was determined as the logarithm of the ratio of concentration of product in octanol and PBS, determined by mass signals.

Solubility. 10µL of a 10 mM solution in DMSO of the compound was diluted either in 490 µL of PBS pH 7.4 or in organic solvent MeOH in a 700 µL-microtube (in triplicate). The tubes were gently shaken 24 h at room temperature, then centrifuged for 5 min at 4000 rpm. The mixtures

were filtered over 0.45 µm filters (Millex-LH Millipore). An amount equal to 20 µL of each solution was added to 180 µL of MeOH and analyzed by LC-MS. The solubility was determined by the ratio of mass signal areas PBS/MeOH.

Metabolic stability. We purchased mouse (CD-1) liver microsomes from BD Gentest. We performed all incubations in duplicate in a shaking water bath at 37 °C. The incubation mixtures contained 10 µM of compound with 1% methanol used as a vehicle, mouse liver microsomes (0.6 mg of microsomal protein per ml), 5 mM $MgCl_2$, 1 mM NADP, 5 mM glucose-6-phosphate, 0.4 $U.mL^{-1}$ glucose-6-phosphate dehydrogenase and 50 mM potassium phosphate buffer (pH 7.4) in a final volume of 1.5 mL. We took samples at 5, 10, 20, 30 and 40 min after microsome addition, and we stopped the reactions by adding ice-cold acetonitrile containing 1 µM internal standard (four volumes). We centrifuged the samples for 10 min at 10000g and 4 °C to pellet precipitated microsomal proteins, and we subjected the supernatant to liquid chromatography–tandem mass spectrometry (LC-MS/MS) analysis. We performed control incubations with denaturated microsomes with acetonitrile containing 1 µM internal standard, and we took samples at the start of the incubation and 40 min later (to evaluate the chemical stability of the compounds in the experimental conditions). Analytes were separated in incubation mixtures by HPLC with a Luna C18(2), 5µm, 50x2.1 mm column (Phenomenex). The mobile phase solvents used were 0.1% formic acid in water (A) or 0.1% formic acid in acetonitrile (B). We applied the following mobile phase gradient: 2–98% (B) for 2.30 min; hold at 98% (B) for 1.00 min; 98-2% (B) for 0.10 min; 2% (B) hold for 1.50 min. The injection volume was 10 µL, and the flow rate was 0.6 $mL.min^{-1}$. We quantified each compound by converting the corresponding analyte/internal standard peak area ratios to percentage drug remaining, using the initial ratio

values in control incubations as 100%. We used propranolol, known as a high hepatic clearance drug in rodents, as a quality-control compound for the microsomal incubations.

Crystal Structure Determination of EthR Ligand Complexes. EthR crystals were produced by the vapour diffusion method as described previously.[22] Crystallization drops were streak seeded. The crystallization buffer contained: 1.4 - 1.65 M Ammonium Sulfate (using 0.05 M increment), 15% Glycerol and 0.1 M MES pH 6.7. The EthR ligand complexes were prepared by mixing 1 µL of ligand (33 mM in 100% DMS0) and 9 µL of the purified protein (9 mg/mL) and equilibrated for 30 minutes at room temperature prior crystallization. Crystals appeared within two days incubation at 20°C. Crystals were flash frozen in liquid nitrogen, using mother liquor supplemented with 15% glycerol as cryoprotectant. The X-ray diffraction data were collected on a Mar CCD mosaic300 detector using synchrotron radiation on PXIII beamline (SLS, PSI, Switzerland). EthR crystals belonged to the space group P_{41212}, with one monomer in the asymmetric unit. Indexing was performed using XDS[23], scaling and merging were performed using the CCP4 package.[24] Structures were refined with the macromolecular refinement program REFMAC5. Initially ligands were fitted into the density using findligand (CCP4), and then manually positioned using Coot[25].

Chemistry.

The chemistry experimental conditions and compounds analysis are detailed in the supporting information.

Associated content.

Supporting information: Chemistry experimental section.

Author information

Corresponding Authors

For B.Villemagne: phone, +33(0)320964991; fax, +33(0)320964709; e-mail, baptiste.villemagne@univ-lille.fr, website U1177, http://www.deprezlab.fr.

For B.Deprez : phone, +33(0)320964924; fax, +33(0)320964709; e-mail, benoit.deprez@univ-lille.fr, website U1177, http://www.deprezlab.fr.

Notes

The authors declare no competing financial interest.

Acknowledgements.

Baptiste Villemagne was recipient of a doctoral fellowship MENR and Ngoc Chau Tran was the recipient of a AUF doctoral fellowship. We are grateful to the institutions that support our laboratories (Inserm, INSERM-Avenir fellowship to Priscille Brodin, Institut Pasteur Korea (Grants : K204EA000001-08E0100-00100 and K204EA000001-09E0100-00100), Univ Lille Nord de France, Institut Pasteur de Lille, CNRS, EU, Région Nord-Pas de Calais, FEDER (N°09220019 and 09220020 PRESAGE 31510), ANR (ANR-06-EMPB-033), PRIM: Pôle de Recherche Interdisciplinaire du Médicament and the European Commission under the 7th Framework Program: Research Infrastructures (Grant Agreement Number 226716)). Financial support to Arnaud Machelart for this work was provided by Fondation pour la Recherche

Medicale (SPF20170938709), the European Community (CycloNHit n° 608407) and the Agence Nationale de la Recherche (ANR-10-EQPX-04-01, ANR-14-CE08-0017, ANR-16-CE35-0009). Diffraction data were collected at the Swiss Light Source (Paul Scherrer Institute, Villigen, Switzerland). We are grateful to the machine and beamline scientists whose outstanding efforts have made these experiments possible. Data management was performed using Pipeline Pilot from Accelrys. We thank VARIAN Inc. for their technical support. NMR acquisitions were done by the LARMN, Lille and SPR acquisitions were done at the molecular interaction platform (IMPRT-IFR114).

Abbreviations used.

ACN: Acetonitrile ; CFU: Colonies forming unit; Cl_{int}: intrinsic clearance; DCE: Dichloroethane; DCM: Dichloromethane; DIEA: Diisopropylethylamine; DMF: Dimethylformamide; ETH: Ethionamide; EtOAc: Ethyl Acetate; HAC: Heay Atoms Count; HBTU: O-(Benzotriazol-1-yl)-N,N,N′,N′-tetramethyluronium hexafluorophosphate; HOBt 1-Hydroxybenzotriazole; LE Ligand Efficiency; MIC Minimal Inhibitory concentration; NAD Nicoatinamide Adenoside Dinucleotide; pCD poly-β-cyclodextrin nanoparticles; RT Room temperature; SEM Standard error of the mean; SPR Surface Plasmon Resonance; TB Tuberculosis; THF Tetrahydrofuran; T_m melting temperature; TMSCl TrimethylSilylchloride; $t_{1/2}$ half life; WHO World Health Organization

References.

1. WHO *Global Tuberculosis Report*; 2018.
2. Villemagne, B.; Crauste, C.; Flipo, M.; Baulard, A. R.; Déprez, B.; Willand, N., Tuberculosis: the drug development pipeline at a glance. *Eur J Med Chem* **2012,** *51*, 1-16.
3. Mohamed Jawed, A.; Mohammad Yousuf, A.; Sabina, Y.; Surender Singh, J.; Pradeep, K.; Shiv Kumar, G.; Ajay Aseri and Habibullah, K., Tuberculosis: Current Treatment, Diagnostics, and Newer Antitubercular Agents in Clinical Trials. *Infectious Disorders - Drug Targets* **2015,** *15* (1), 32-41.
4. Willand, N.; Dirie, B.; Carette, X.; Bifani, P.; Singhal, A.; Desroses, M.; Leroux, F.; Willery, E.; Mathys, V.; Deprez-Poulain, R.; Delcroix, G.; Frenois, F.; Aumercier, M.; Locht, C.; Villeret, V.; Deprez, B.; Baulard, A. R., Synthetic EthR inhibitors boost antituberculous activity of ethionamide. *Nat Med* **2009,** *15* (5), 537-544.
5. Blondiaux, N.; Moune, M.; Desroses, M.; Frita, R.; Flipo, M.; Mathys, V.; Soetaert, K.; Kiass, M.; Delorme, V.; Djaout, K.; Trebosc, V.; Kemmer, C.; Wintjens, R.; Wohlkönig, A.; Antoine, R.; Huot, L.; Hot, D.; Coscolla, M.; Feldmann, J.; Gagneux, S.; Locht, C.; Brodin, P.; Gitzinger, M.; Déprez, B.; Willand, N.; Baulard, A. R., Reversion of antibiotic resistance in Mycobacterium tuberculosis by spiroisoxazoline SMARt-420. *Science* **2017,** *355* (6330), 1206-1211.
6. Vannelli, T. A.; Dykman, A.; Ortiz de Montellano, P. R., The Antituberculosis Drug Ethionamide Is Activated by a Flavoprotein Monooxygenase. *Journal of Biological Chemistry* **2002,** *277* (15), 12824-12829.
7. Baulard, A. R.; Betts, J. C.; Engohang-Ndong, J.; Quan, S.; Brennan, P. J.; Locht, C.; Besra, G. S., Activation of the pro-drug ethionamide is regulated in mycobacteria. *Journal of Biological Chemistry* **2000**.
8. DeBarber, A. E.; Mdluli, K.; Bosman, M.; Bekker, L.-G.; Barry, C. E., Ethionamide activation and sensitivity in multidrug-resistant Mycobacterium tuberculosis. *Proceedings of the National Academy of Sciences* **2000,** *97* (17), 9677-9682.
9. Flipo, M.; Willand, N.; Lecat-Guillet, N.; Hounsou, C.; Desroses, M.; Leroux, F.; Lens, Z.; Villeret, V.; Wohlkönig, A.; Wintjens, R.; Christophe, T.; Kyoung Jeon, H.; Locht, C.; Brodin, P.; Baulard, A. R.; Déprez, B., Discovery of Novel N-Phenylphenoxyacetamide Derivatives as EthR Inhibitors and Ethionamide Boosters by Combining High-Throughput Screening and Synthesis. *Journal of Medicinal Chemistry* **2012,** *55* (14), 6391-6402.
10. Flipo, M.; Desroses, M.; Lecat-Guillet, N.; Dirié, B.; Carette, X.; Leroux, F.; Piveteau, C.; Demirkaya, F.; Lens, Z.; Rucktooa, P.; Villeret, V.; Christophe, T.; Jeon, H. K.; Locht, C.; Brodin, P.; Déprez, B.; Baulard, A. R.; Willand, N., Ethionamide Boosters: Synthesis, Biological Activity, and Structure−Activity Relationships of a Series of 1,2,4-Oxadiazole EthR Inhibitors. *Journal of Medicinal Chemistry* **2011,** *54* (8), 2994-3010.
11. Flipo, M.; Desroses, M.; Lecat-Guillet, N.; Villemagne, B.; Blondiaux, N.; Leroux, F.; Piveteau, C.; Mathys, V.; Flament, M.-P.; Siepmann, J.; Villeret, V.; Wohlkönig, A.; Wintjens, R.; Soror, S. H.; Christophe, T.; Jeon, H. K.; Locht, C.; Brodin, P.; Déprez, B.; Baulard, A. R.; Willand, N., Ethionamide Boosters. 2. Combining Bioisosteric Replacement and Structure-Based Drug Design To Solve Pharmacokinetic Issues in a Series of Potent 1,2,4-Oxadiazole EthR Inhibitors. *Journal of Medicinal Chemistry* **2011,** *55* (1), 68-83.
12. Mendes, V.; Blundell, T. L., Targeting tuberculosis using structure-guided fragment-based drug design. *Drug Discovery Today* **2017,** *22* (3), 546-554.

13. Marchetti, C.; Chan, D. S. H.; Coyne, A. G.; Abell, C., Fragment-based approaches to TB drugs. *Parasitology* **2018,** *145* (2), 184-195.
14. Lamoree, B.; Hubbard, R. E., Using Fragment-Based Approaches to Discover New Antibiotics. *SLAS Discov* **2018,** *23* (6), 495-510.
15. Moreira, W.; Lim, J. J.; Yeo, S. Y.; Ramanujulu, P. M.; Dymock, B. W.; Dick, T., Fragment-Based Whole Cell Screen Delivers Hits against M. tuberculosis and Non-tuberculous Mycobacteria. *Frontiers in Microbiology* **2016,** *7*, 1392.
16. Nikiforov, P. O.; Surade, S.; Blaszczyk, M.; Delorme, V.; Brodin, P.; Baulard, A. R.; Blundell, T. L.; Abell, C., A fragment merging approach towards the development of small molecule inhibitors of Mycobacterium tuberculosis EthR for use as ethionamide boosters. *Org Biomol Chem* **2016,** *14* (7), 2318-26.
17. Nikiforov, P. O.; Blaszczyk, M.; Surade, S.; Boshoff, H. I.; Sajid, A.; Delorme, V.; Deboosere, N.; Brodin, P.; Baulard, A. R.; Barry, C. E.; Blundell, T. L.; Abell, C., Fragment-Sized EthR Inhibitors Exhibit Exceptionally Strong Ethionamide Boosting Effect in Whole-Cell Mycobacterium tuberculosis Assays. *ACS Chem Biol* **2017,** *12* (5), 1390-1396.
18. Surade, S.; Ty, N.; Hengrung, N.; Lechartier, B.; Cole, Stewart T.; Abell, C.; Blundell, Tom L., A structure-guided fragment-based approach for the discovery of allosteric inhibitors targeting the lipophilic binding site of transcription factor EthR. *Biochemical Journal* **2014,** *458* (2), 387.
19. Shiu-Hin Chan, D.; Seetoh, W.-G.; McConnell, B. N.; Matak-Vinković, D.; Thomas, S. E.; Mendes, V.; Blaszczyk, M.; Coyne, A. G.; Blundell, T. L.; Abell, C., Structural insights into the EthR–DNA interaction using native mass spectrometry. *Chemical Communications* **2017,** *53* (25), 3527-3530.
20. Chan, D. S.; Mendes, V.; Thomas, S. E.; McConnell, B. N.; Matak-Vinković, D.; Coyne, A. G.; Blundell, T. L.; Abell, C., Fragment Screening against the EthR-DNA Interaction by Native Mass Spectrometry. *Angew Chem Int Ed Engl* **2017,** *56* (26), 7488-7491.
21. Villemagne, B.; Flipo, M.; Blondiaux, N.; Crauste, C.; Malaquin, S.; Leroux, F.; Piveteau, C.; Villeret, V.; Brodin, P.; Villoutreix, B. O.; Sperandio, O.; Soror, S. H.; Wohlkönig, A.; Wintjens, R.; Deprez, B.; Baulard, A. R.; Willand, N., Ligand Efficiency Driven Design of New Inhibitors of Mycobacterium tuberculosis Transcriptional Repressor EthR Using Fragment Growing, Merging, and Linking Approaches. *Journal of Medicinal Chemistry* **2014,** *57* (11), 4876-4888.
22. Campbell, T. F.; Stephens, C. E., Nuclear fluorination of 2,4-diarylthiazoles with Accufluor®. *Journal of Fluorine Chemistry* **2006,** *127* (12), 1591-1594.
23. Augustine, J. K.; Vairaperumal, V.; Narasimhan, S.; Alagarsamy, P.; Radhakrishnan, A., Propylphosphonic anhydride (T3P®): an efficient reagent for the one-pot synthesis of 1,2,4-oxadiazoles, 1,3,4-oxadiazoles, and 1,3,4-thiadiazoles. *Tetrahedron* **2009,** *65* (48), 9989-9996.
24. Legros, J.-Y.; Primault, G.; Fiaud, J.-C., Syntheses of acetylquinolines and acetylisoquinolines via palladium-catalyzed coupling reactions. *Tetrahedron* **2001,** *57* (13), 2507-2514.
25. Zhang, H.-Z.; Kasibhatla, S.; Kuemmerle, J.; Kemnitzer, W.; Ollis-Mason, K.; Qiu, L.; Crogan-Grundy, C.; Tseng, B.; Drewe, J.; Cai, S. X., Discovery and Structure−Activity Relationship of 3-Aryl-5-aryl-1,2,4-oxadiazoles as a New Series of Apoptosis Inducers and Potential Anticancer Agents. *Journal of Medicinal Chemistry* **2005,** *48* (16), 5215-5223.

26. Talele, T. T., The "Cyclopropyl Fragment" is a Versatile Player that Frequently Appears in Preclinical/Clinical Drug Molecules. *Journal of Medicinal Chemistry* **2016,** *59* (19), 8712-8756.
27. Costa-Gouveia, J.; Pancani, E.; Jouny, S.; Machelart, A.; Delorme, V.; Salzano, G.; Iantomasi, R.; Piveteau, C.; Queval, C. J.; Song, O.-R.; Flipo, M.; Deprez, B.; Saint-André, J.-P.; Hureaux, J.; Majlessi, L.; Willand, N.; Baulard, A.; Brodin, P.; Gref, R., Combination therapy for tuberculosis treatment: pulmonary administration of ethionamide and booster co-loaded nanoparticles. *Scientific Reports* **2017,** *7* (1), 5390.
28. Kurkov, S. V.; Loftsson, T., Cyclodextrins. *International Journal of Pharmaceutics* **2013,** *453* (1), 167-180.
29. Salzano, G.; Wankar, J.; Ottani, S.; Villemagne, B.; Baulard, A. R.; Willand, N.; Brodin, P.; Manet, I.; Gref, R., Cyclodextrin-based nanocarriers containing a synergic drug combination: A potential formulation for pulmonary administration of antitubercular drugs. *International Journal of Pharmaceutics* **2017**.

Tables

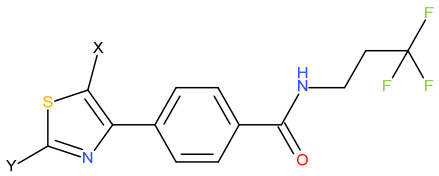

Cpd	Y	X	ΔT_m (°C)[a]	EC_{50} (µM)[b]	HA[c]	LE[d]
3	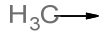	H	10.6	0.10	21	0.46
4	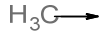	F	n.t.	0.055	22	0.45
5	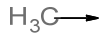	Cl	8.7	>2.5	22	-
6	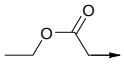	H	10.1	0.58	26	0.33
7	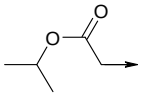	H	13.2	0.10	27	0.36
8	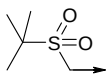	H	9.6	0.25	28	0.32
9	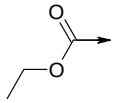	H	9.6	>2.5	25	-
10	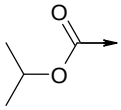	H	8.2	>2.5	26	-
11	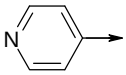	H	12.6	0.072	26	0.38

12	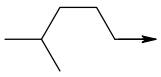	H	13.0	0.43	26	0.34
13		H	12.6	0.049	24	0.42
14		H	8.1	>2.5	20	-

Table 1. **Biological activities of compounds 4-14.** [a]ΔTm data were obtained using thermal shift assay. [b]EC_{50} represents the concentration of ligand that allows ethionamide at 0.1 µg/mL (normal MIC/10) to inhibit 50% of *M. tuberculosis* growth in macrophages. [c]HA = number of non-hydrogen atoms. [d]LE = -1.37log(EC_{50})/HA

	Biological activity			Physicochemical properties		
Compound	ΔT_m (°C)[a]	EC_{50} (µM)[b]	LE[c]	HA[d]	logD[e]	Solubility (µg/mL)[f]
3	10.6	0.10	0.46	21	2.8	14.7
4	-	0.055	0.45	22	3.2	10.6
13	12.6	0.049	0.42	24	3.9	1.6

Table 2. **Biological activities, Physicochemical and pharmacokinetic properties of compounds 3, 4, 13.** [a]ΔTm data were obtained using thermal shift assay. [b]EC_{50} represents the concentration of ligand that allows ethionamide at 0.1 µg/mL (normal MIC/10) to inhibit 50% of *M. tuberculosis* growth in macrophages. [c]LE = -1.37log(EC_{50})/HA. [d]HA = number of non-hydrogen atoms.[e] LogD were measured at pH 7.4 between PBS and octanol. [f]Solubilities were determined at pH 7.4.

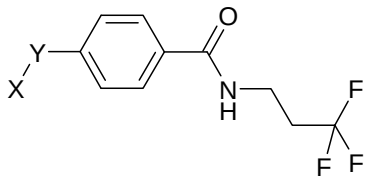

Cpd	X	Y	ΔT_m (°C)[a]	EC_{50} (μM)[b]	HA[c]	LE[d]
3	H_3C→	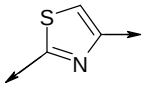	10.6	0.10	21	0.46
15	H_3C→	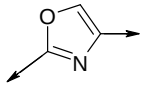	7.8	0.28	21	0.43
16	H_3C→	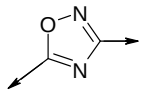	9.3	0.08	21	0.46
17	H_3C→	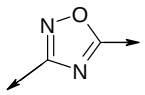	7.9	0.26	21	0.43
18	H_3C→	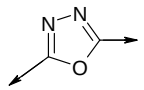	4.3	>2.5	21	-
19	H_3C→	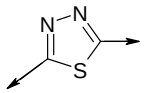	4.8	>2.5	21	-
20	H_3C→	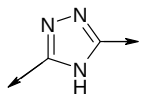	1.9	>2.5	21	-
21		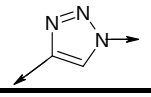	3.6	>2.5	24	-

Table 3 Biological activities of compounds 15-21. [a]ΔTm data were obtained using thermal shift assay. [b]EC_{50} represents the concentration of ligand that allows ethionamide at 0.1 μg/mL (normal MIC/10) to inhibit 50% of *M. tuberculosis* growth in macrophages. [c]HA = number of non-hydrogen atoms. [d]LE = -1.37log(EC_{50})/HA

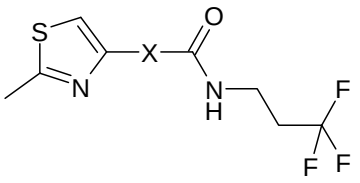

Cpd	X	ΔT_m (°C)[a]	EC_{50} (µM)[b]	HA[c]	LE[d]
22	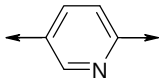	10.0	0.17	21	0.44
23	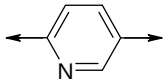	6.1	1.0	21	0.39

Table 4. **Biological activities of compounds 22-23.** [a]ΔTm data were obtained using thermal shift assay. [b]EC_{50} represents the concentration of ligand that allows ethionamide at 0.1 µg/mL (normal MIC/10) to inhibit 50% of *M. tuberculosis* growth in macrophages. [c]HA = number of non-hydrogen atoms. [d]LE = -1.37log(EC_{50})/HA

	Biological activity			Physicochemical properties			Pharmacokinetics	
Compound	ΔT_m (°C)[a]	EC_{50} (µM)[b]	LE[c]	HA[d]	logD[e]	Solubility (µg/mL)[f]	$t_{1/2}$ microsomes (min)[g]	Cl (µL.min^{-1}.mg^{-1})[h]
3	10.6	0.10	0.46	21	2.8	14.7	10	144
16	9.3	0.082	0.46	21	2.3	21.8	7	172
22	10.0	0.17	0.44	21	2.5	61.1	6	216

Table 5. **Biological activities, physicochemical and pharmacokinetic properties of compounds 3, 16 and 22.** [a]ΔTm data were obtained using thermal shift assay. [b]EC_{50} represents the concentration of ligand that allows ethionamide at 0.1 µg/mL (normal MIC/10) to inhibit 50% of *M. tuberculosis* growth in macrophages. [c]LE = -1.37log(EC_{50})/HA. [d]HA = number of non-hydrogen atoms. [e]LogD were measured at pH 7.4 between PBS and octanol. [f]Solubilities were determined at pH 7.4. [g] Propranolol, known as a high hepatic clearance drug in rodents, was used as reference for microsomal incubations ($t_{1/2}$ = 13 min, CL_{int} = 121 µL.min^{-1}.mg^{-1}). [h]All

compounds have been tested at the same concentration (1 µM). The values given here should not be read as bona fide clearance values but as indicators to rank compounds according to metabolic stability.

Cpd	Structure	Biological activity			Physicochemical properties		Pharmacokinetics	
		ΔT_m (°C)[a]	EC_{50} (µM)[b]	LE[c]	logD[d]	Solubility (µg/mL)[e]	$t_{1/2}$ (min)[f]	Cl (µL.min^{-1}.mg^{-1})[g]
3	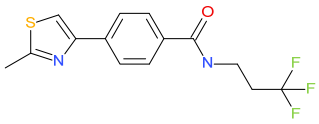	10.6	0.10	0.46	2.8	14.7	10	144
24	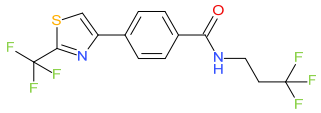	9.9	0.10	0.40	3.6	8.2	19	62
25	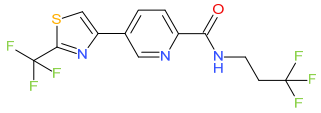	9.5	0.098	0.40	3.3	17.2	16	79
26	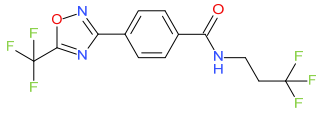	10.2	0.073	0.41	3.5	2.4	22	57
27	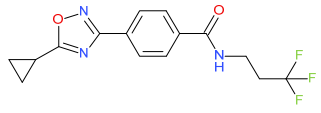	10.2	0.072	0.43	3.1	9.9	19	69
28	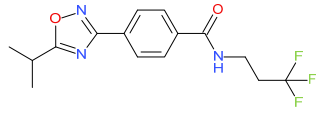	11.3	0.065	0.43	3.3	17.1	6	229

Table 6. Biological activities, physicochemical and pharmacokinetic properties of compounds 24-28. [a]ΔTm data were obtained using thermal shift assay. [b]EC_{50} represents the

concentration of ligand that allows ethionamide at 0.1 µg/mL (normal MIC/10) to inhibit 50% of *M. tuberculosis* growth in macrophages. [c]LE = -1.37log(EC_{50})/HA. [d] LogD were measured at pH 7.4 between PBS and octanol. [e]Solubilities were determined at pH 7.4. [f] Propranolol, known as a high hepatic clearance drug in rodents, was used as reference for microsomal incubations ($t_{1/2}$ = 13 min, CL_{int} = 121 µL.min^{-1}.mg^{-1}). [g]All compounds have been tested at the same concentration (1 µM). The values given here should not be read as bona fide clearance values but as indicators to rank compounds according to metabolic stability.

Figures

Figure 1. **Structures of previously developed fragment-based EthR inhibitors 1, 2 and 3.**

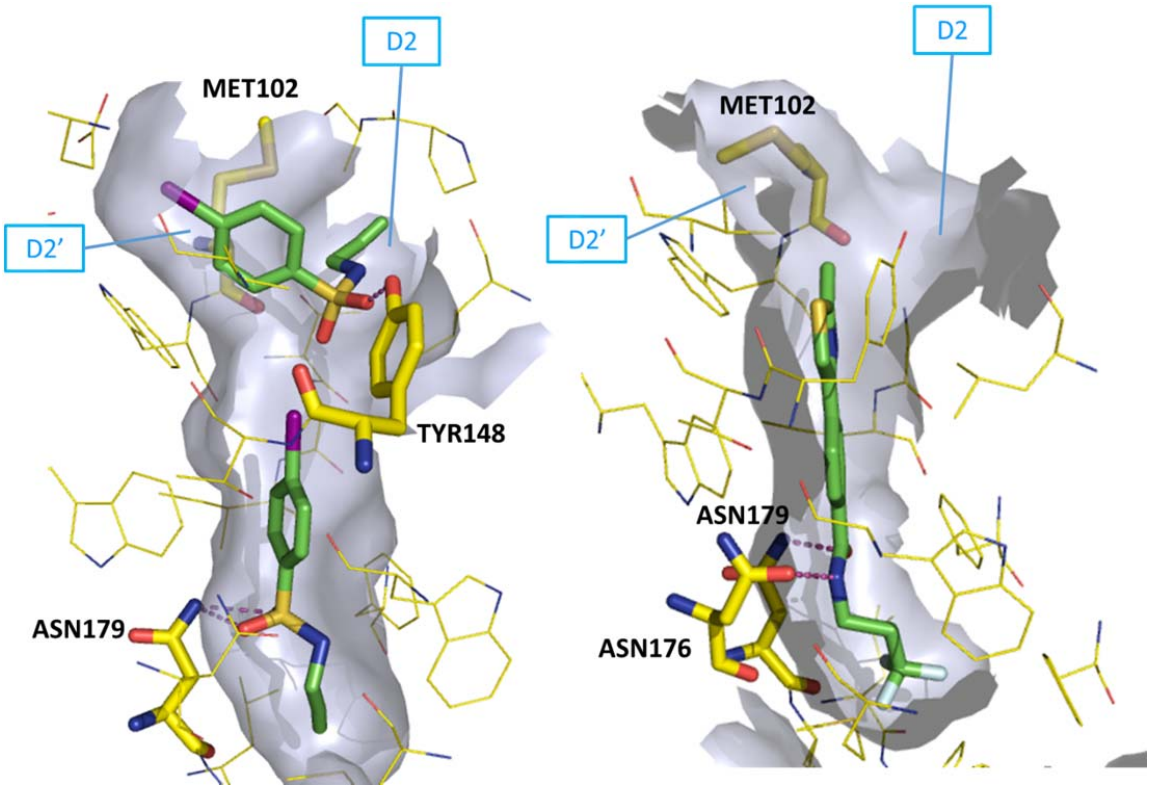

Figure 2. **Binding mode of fragment 1 (left, PDB ID ??, resolution 2.0 Å) and compound 3 (right, PDB ID 4M3B, resolution 2.0 Å) to EthR.**

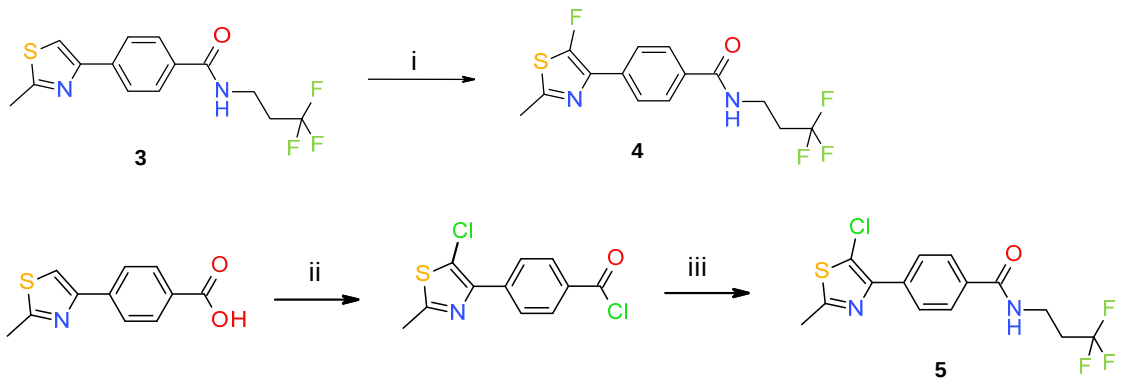

Figure 3. **Synthesis of halogenated compounds 4 and 5.** Reagents and reaction conditions: (i) Selectfluor (2.5eq.), anhydrous DMF, 0°C to RT, 55 h; (ii) $SOCl_2$, 50°C, 6 h; (iii) 3,3,3-trifluoropropylamine hydrochloride (1.1eq.), DIEA (4eq.), DCM, RT, overnight.

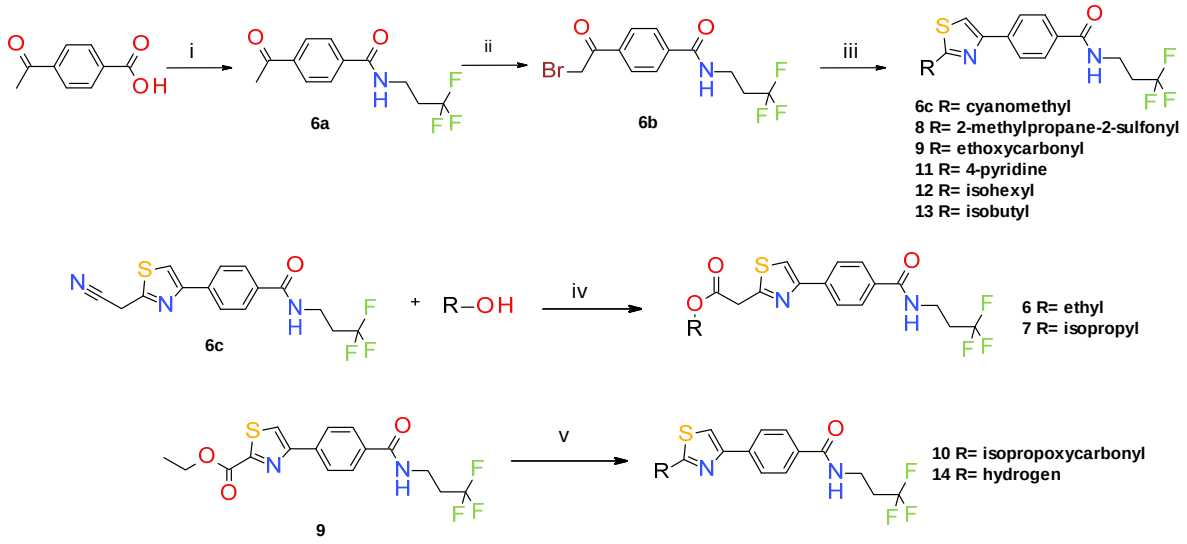

Figure 4. Synthesis of compounds 6-14. Reagents and reaction conditions : (i) 4-acetylbenzoic acid (1eq.), DIEA (4eq.), HBTU (1.2eq.), HOBt (0.2eq.), 3,3,3-trifluoropropylamine hydrochloride (1eq.), anhydrous DMF, RT, 2 h; (ii) trimethylphenylammonium tribromide

(1.55eq.), DCE / MeOH (5/2), 50°C, 3 h; (iii) thioamide (1-1.4eq.), THF, reflux, 3-48 h; (iv) Anhydrous alcohol (48-59eq.), TMSCl (14-24eq.), H_2O (0-1eq.) 40°C, 4-16 h; (v) (a) Sodium (5.8 eq.), isopropanol, reflux, overnight, (b) $SOCl_2$, 50°C, overnight.

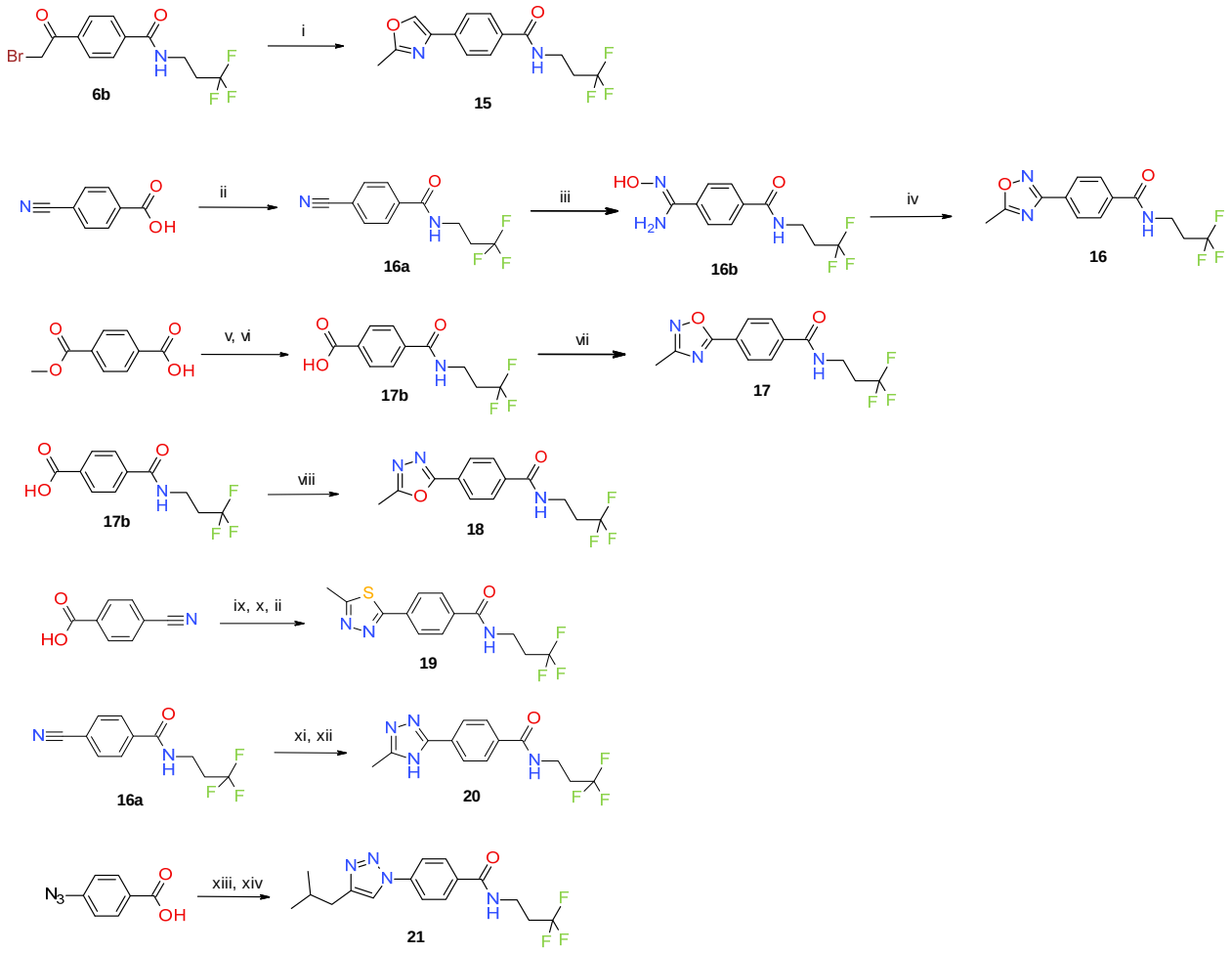

Figure 5. **Synthesis of analogs 15 to 21.** Reagents and reaction conditions: (i) Acetamide (1.2eq.), Toluene, 110°C, 10 min, µW irradiation; (ii) 3,3,3-trifluoropropylamine hydrochloride (1eq.), T3P® 50% w/w EtOAc (1.2-1.7eq.), DIEA (3-4eq.), EtOAc, RT, overnight; (iii)

Hydroxylamine hydrochloride (1.5eq.), DIEA (1.6eq.), EtOH, reflux, 2 h; (iv) Acetic acid (1.1eq.), T3P® 50% w/w EtOAc (3eq.), DIEA (3.5eq.), EtOAc, reflux, 60 h; (v) 3,3,3-trifluoropropylamine hydrochloride (1eq.), HBTU (1.2eq.), HOBt (0.2eq.), DIEA (4eq.), DMF, RT, 1 h; (vi) KOH (4eq.), MeOH, reflux, 2 h; (vii) Acetamide oxime (1eq.), T3P® 50% w/w EtOAc (4.2eq.), DIEA (4eq.), EtOAc, reflux, 36 h; (viii) Acetylhydrazine (1.1eq.), T3P® 50% w/w EtOAc (4.2eq.), DIEA (4eq.), EtOAc, reflux, 72 h; (ix) Lawesson's reagent (1.75eq.), Acetylhydrazine (1eq.), T3P® 50% w/w EtOAc (1.75eq.), DIEA (2.5eq.), EtOAc, reflux, overnight; (x) 10% aq NaOH, reflux, 1 h; (xi) 4N HCl in dioxane, MeOH, 0°C to TA, overnight; (xii) DIEA (1.5eq.), EtOH, RT, 15 min. Then acetylhydrazine (1 eq.), reflux, 60 h; (xiii) 3,3,3-trifluoropropylamine hydrochloride (1eq.), HOBt (0.57eq.), HBTU (1.2eq.), DIEA (4eq.), DMF, RT, overnight; (xiv) 4-methylpentyne (2eq.), $CuSO_4$ (0.15eq.), sodium ascorbate (1.5eq.), t-BuOH/H_2O 1/1, RT, overnight.

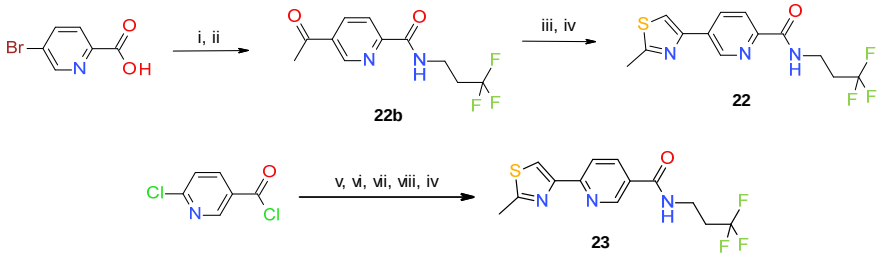

Figure 6. **Synthesis of analogs 22 and 23.** Reagents and reaction conditions: (i) 3,3,3-trifluoropropylamine hydrochloride (1eq.), T3P® 50% w/w EtOAc (1.2eq.), DIEA (3eq.), EtOAc, RT, 3 h; (ii) $PdCl_2(PPh_3)_2$ (0.1eq.), toluene, RT, 5 min. Tributyl(1-ethoxyvinyl)tin (1.2eq.), 90°C, overnight. 1N aq HCl, RT, 1 h; (iii) trimethylphenylammonium tribromide (1eq.), DCE / MeOH (5/2), 70°C, 24-72 h; (iv) Thioacetamide (1-1.5eq.) EtOH, reflux, 3-4 h; (v) 3,3,3-

trifluoropropylamine hydrochloride (1eq.), N-methylmorpholine (4eq.), DCM, RT, overnight; (vi) Acetyl chloride (0.2eq.), sodium iodide (5eq.), acetonitrile, 105°C, overnight; (vii) $PdCl_2(PPh_3)_2$ (0.1eq.), toluene, RT, 5 min. Tributyl(1-ethoxyvinyl)tin (1.2eq.), 90°C, overnight. 1N aq HCl, RT, 1 h.

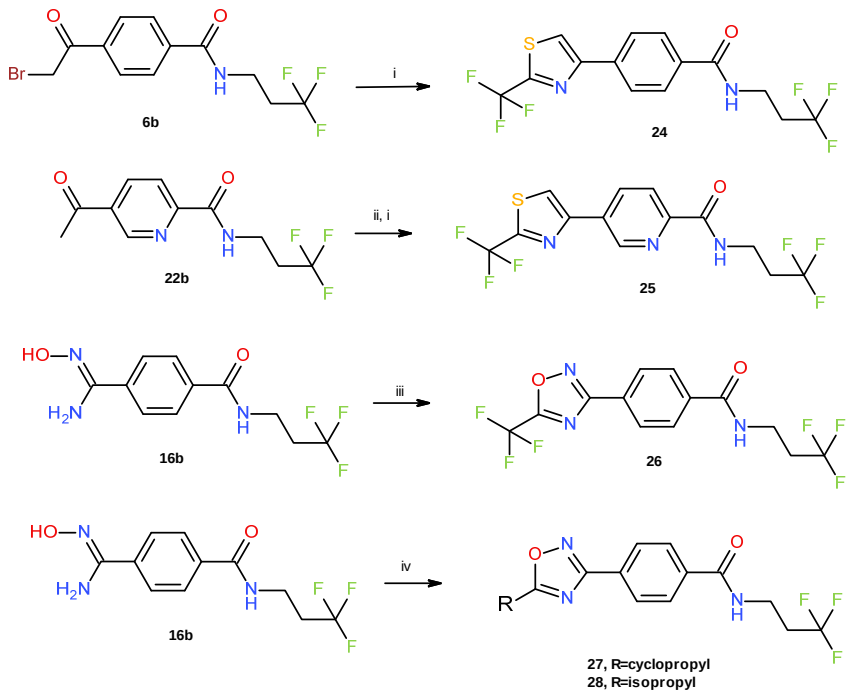

Figure 7. **Synthesis of analogs 24 to 28.** Reagents and reaction conditions: (i) 2,2,2-trifluorothioacetamide (2.5-2.7 eq.), ACN, 81-96 h, reflux; (ii) trimethylphenylammonium tribromide (1.1 eq.), DCE / MeOH (5/2), 65°C, overnight; (iii) Trifluoroacetic acid (1.1 eq.), T3P® 50% w/w DMF (3eq.), DIEA (3eq.), DMF, 80 °C, 114 h; (iv) Carboxylic acid (2.7-3.2 eq.), T3P® 50% w/w DMF (5.2-6.2 eq.), DIEA (6.2-7.2 eq.), EtOAc, reflux, 114h.

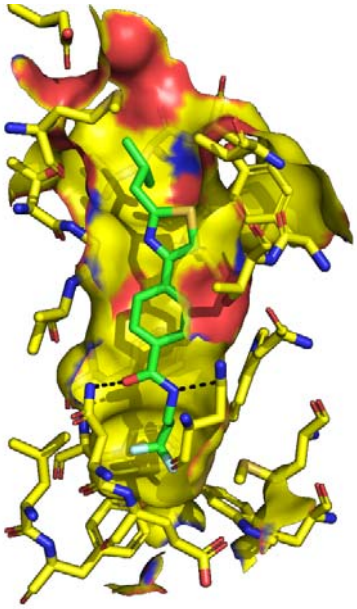

Figure 8. **Binding mode of compound 13 to EthR (PDB ID 6HO4, resolution 1.6 Å)**

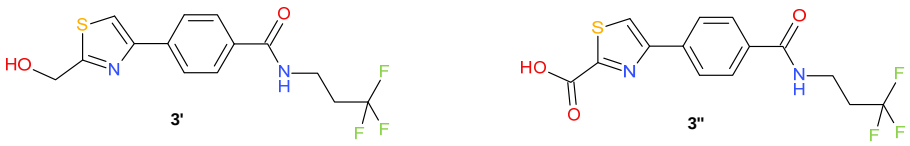

Figure 9. **Structure of compounds 3’ and 3’’.**

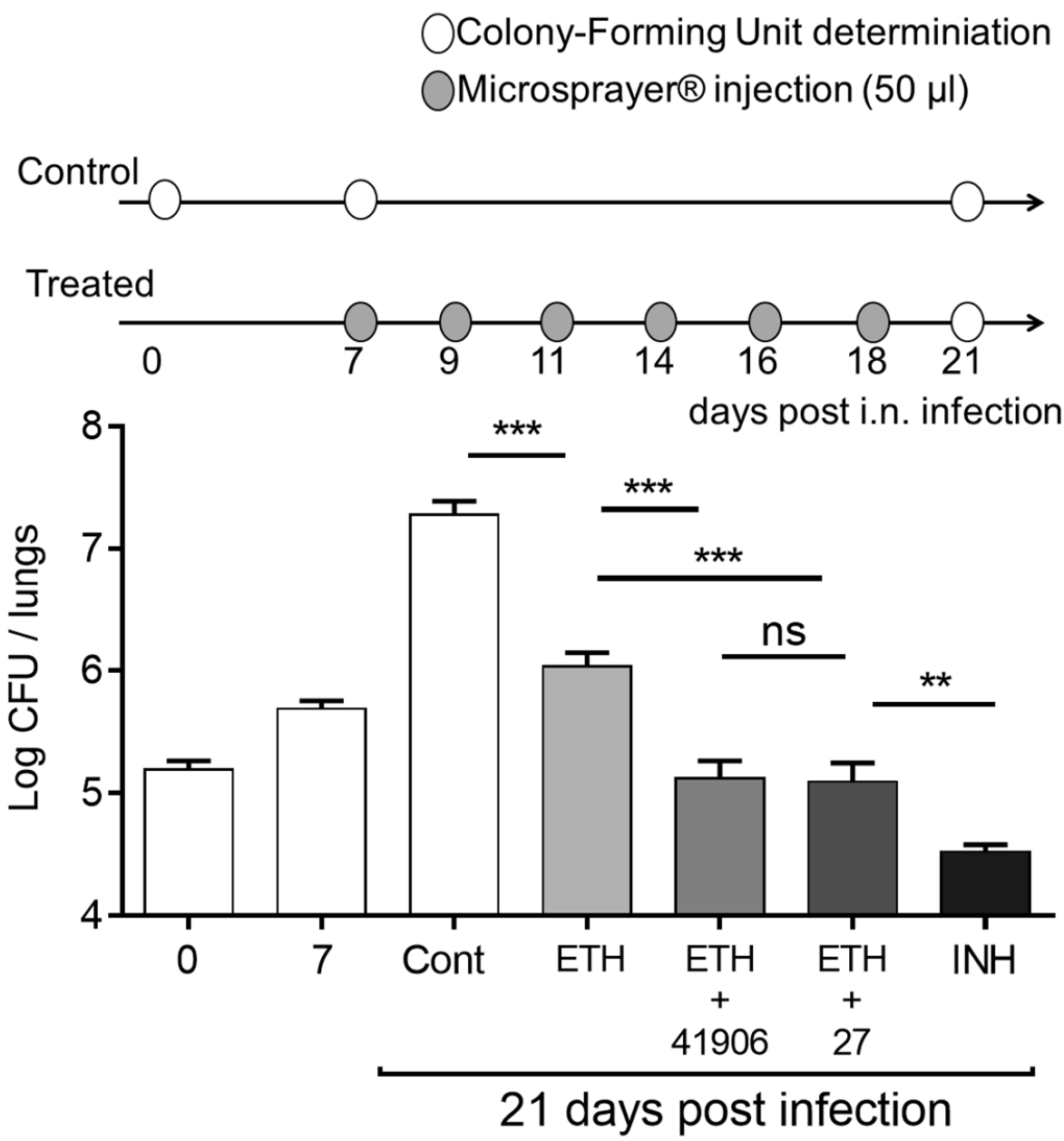

Figure 10. **Ethionamide boosting effect of BDM41906 and compound 27 on TB-infected mice.** 7 days after infection, mice were treated for 2 weeks, 3 times per week with ETH, ETH+BDM41906, ETH+27 at 4 mg/mL in 200 mg/mL pCD solutions, or INH at 4 mg/mL. The mice were then killed and the pulmonary bacillary load was enumerated by CFUs. Values are

means of at least 3 mice per group. Data are presented as mean ± SEM and are representative of at least two independent experiments. Values of $p < 0.05$ were considered to represent a significant difference. **, and *** denote $p < 0.01$, and $p < 0.001$, respectively.

Table of Contents Graphic.